

Height Quantized Diffractive Deep Neural Networks

Runze Li^{a,b}, Xuhui Zhuang^c, Gege Ding^d, Mingzhu Song^c, Guang Jin^{a,b}, Xuemin Zhang^{a,b}, Jie Wen^{d,e}, Shaoju Wang^{a,b,*}

^a*School of Remote Sensing and Information Engineering, Wuhan University, Wuhan, 430072, China*

^b*The Research Institute of Aerospace Science and Technology, Wuhan University, Wuhan, 430072, China*

^c*Department of Information Science and Technology, Dalian Maritime University, Dalian, 116026, China*

^d*China Waterborne Transport Research Institute, Beijing, 100000, China*

^e*Electronic Information School, Wuhan University, Wuhan, 430072, China*

Abstract

Diffractive deep neural networks (D²NN) have shown advantages in artificial intelligence image processing tasks, such as lens-free imaging. Since the accuracy and resolution of current fabrication technologies such as photolithography and 3D printing are difficult to meet the low-cost D²NN manufacturing, in order to solve this problem, we designed height quantized diffractive deep neural networks, thereby improving the networks detail resolution and reducing the fabrication accuracy requirements. We experimentally verified the functionality of the proposed networks, and simulation results show that this structure can achieve the same training effect with less training time. In addition, the quantization process is introduced into D²NN as a kind of noise, which can partially avoid the overfitting of the diffractive networks.

1. Introduction

Deep learning technology has developed rapidly in the past decades and has achieved incredible achievements in various fields such as image recognition, disease detection, and natural language processing[1–3]. The traditional electronic deep learning neural networks are limited by the von Neumann architecture, and the training process is highly energy and resource consuming[4]. Since optical computing has the characteristics of high bandwidth, high-speed computing, high parallelism and low power consumption compared to electronic neural networks, optical neural networks have unique advantages such as high interconnection speed, wide bandwidth and the ability to process images directly[5–11]. So far, two kinds of optical neural networks have been proposed. The first relies on silicon photonics, which is used to implement matrix multiplication on an optical on-chip platform consisting of multiple Mach-Zender interferometers[12–14]. The other is to collaboratively perform relatively complex optical transformations through diffraction by fabricating a set of diffraction surfaces spaced apart from each other with certain functions[15–21]. As demonstrated, D²NN through diffraction surfaces have great computing

*Corresponding author

Email address: wangshaoju@whu.edu.cn (Shaoju Wang)

1
2 processing capability and reconfigurability, and can effectively achieve typical linear
3 and nonlinear transformations at the speed of light to complete specific tasks.
4

5 Recent developments in materials science and nanophononics provide a pathway
6 for the design and fabrication of D²NN[22, 23]. Mainstream fabrication methods in-
7 clude 3D printing and photolithography. Photolithography can only etch a certain
8 depth at a time. If the D²NN height parameters are not restricted, the height value
9 of each neuron may be different, which will greatly increase the difficulty of pho-
10 tolithography. The 3D printer is programmed to print each neuron independently,
11 so the neuron height parameter is limited only by the accuracy of the printer. The-
12 oreoretically, structures of any height can be printed within the processing accuracy.
13 However, the processing accuracy and size contradiction of current 3D printers are
14 difficult to reconcile. The higher the accuracy of the 3D printer, the longer it takes
15 to process the same device, which is difficult to meet the large-scale, high-precision
16 production of D²NN.
17

18 In order to reduce the fabrication accuracy required for D²NN, in this paper, we
19 designed a training method for height quantized diffractive deep neural networks
20 (HQ-D²NN) and demonstrated the performance of HQ-D²NN with quantization
21 values of 2, 3 and 4, namely HQ₂-D²NN, HQ₃-D²NN and HQ₄-D²NN respectively.
22 In addition, through various numerical evaluations, we demonstrate that HQ-D²NN
23 can be adjusted the number of quantization value according to the complexity of the
24 actual task and the level of fabrication accuracy, which greatly reduces the difficulty
25 of fabrication and the cost of training time while ensuring accuracy.
26
27

30 2. PROPOSED METHOD

31 D²NN is an all-optical machine learning framework. It consists of a stack of
32 multiple optical diffraction layers. Each diffraction layer is composed of a certain
33 number of diffraction gratings that function as artificial neurons. The function of a
34 diffraction grating is to output a phase/amplitude modulated secondary wave. As
35 shown in formula (1), diffraction light follows the Rayleigh-Sommerfeld diffraction
36 formula between the successive diffraction layers. The diffraction light emitted by
37 the diffraction gratings of each layer is considered as a new diffraction light source
38 that propagates forward.
39

$$42 \quad W_i^l(x, y, z) = \frac{z - z_i}{r^2} \left(\frac{1}{2\pi r} + \frac{1}{j\lambda} \right) \exp\left(\frac{j2\pi r}{\lambda}\right) \quad (1)$$

43 Where, W_i^l refers to the light field output by the i-th diffraction grating located
44 at (x_i, y_i, z_i) of the l-th diffraction layer, $r = \sqrt{(x - x_i)^2 + (y - y_i)^2 + (z - z_i)^2}$, λ is
45 the illumination wavelength. Incident light is modulated as it passes through the
46 diffraction grating, and the modulation of light waves can be described as follows:
47

$$52 \quad t_i^l(x, y, z) = W_i^l(x, y, z) \alpha_i^l(x_i, y_i, z_i) \exp(j\Phi_i^l(x_i, y_i, z_i)) \quad (2)$$

53 Where, $\alpha_i^l(x_i, y_i, z_i) \exp(j\Phi_i^l(x_i, y_i, z_i))$ is the complex-value modulation coeffi-
54 cient of the i-th diffraction grating, both amplitude and phase coefficients can be
55 obtained by training. For a phase-only diffractive networks architecture, the ampli-
56 tude value $\alpha_i^l(x_i, y_i, z_i)$ is assumed to be a constant, and the phase value $\Phi_i^l(x_i, y_i, z_i)$
57 limited to 0-2π. Phase modulation is achieved by adjusting the height of the diffrac-
58 tion grating, and its mapping relationship is written as:
59

$$\Delta z = \frac{\lambda\Phi}{2\pi \Delta n} \quad (3)$$

Where, Δz refers to the height of the diffraction grating, λ is the illumination wavelength, ϕ is phase value, and Δn is the refractive index difference between the 3D printing material and air.

Furthermore, the D²NN continuously iterates each diffraction grating modulation parameter during training to improve performance. As shown in Fig. 1, since the diffraction gratings are independent of each other and the phase modulation coefficient can theoretically be any value from 0 to 2π , according to formula (3), the height of the diffraction gratings is randomly distributed and the accuracy values can vary greatly. This makes the manufacturing of the diffractive networks very difficult. Therefore, in order to reduce the manufacturing difficulty, we limit the diffraction grating to a few definite height values, i.e., only a few definite values of the phase modulation coefficient are allowed during the training process.

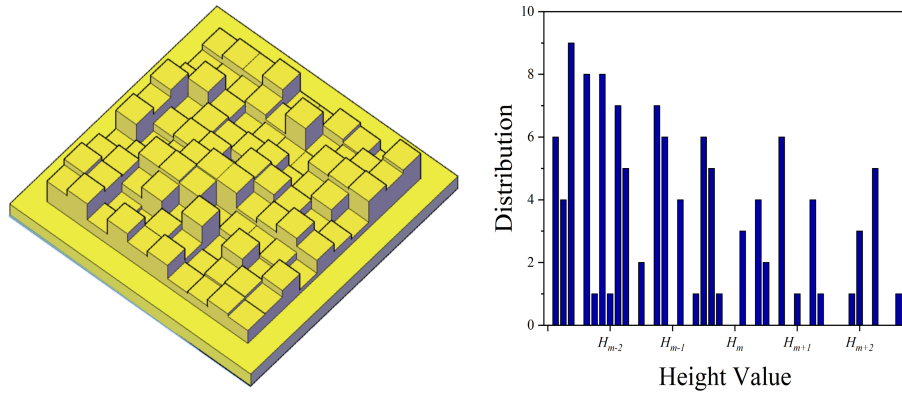


Figure 1: D²NN structure diagram and phase value distribution. Each diffraction grating has an independent height.

3. Architecture of the HQ-D²NN

The accuracy and resolution of commonly used D²NN fabrication equipment such as 3D printers are generally only on the order of 0.01mm and 0.1mm, and the printing speed is about 1mm height/min, which is difficult to meet the increasingly higher integration and precision requirements for D²NN. Since the phase modulation range of the diffraction grating is $[0, 2\pi]$, according to formula (3), the height of the diffraction grating has a maximum value H_{max} . Combined with the height resolution δ of the fabrication equipment, the maximum quantization level Q_{max} can be achieved.

$$Q_{max} = \text{round}\left(\frac{H_{max}}{\delta}\right) \quad (4)$$

Where, $\text{round}()$ refers to round down. The height of each diffraction grating in the diffractive networks can be quantitatively constrained by using linear combinations of different quantization levels Q ($Q \leq Q_{max}$) and δ . And then every diffraction grating quantized height value with the best performance can be obtained through quantified phase modulation coefficient ϕ_Q iterative training phase modulation coefficient ϕ . The mapping relationship of ϕ_Q and ϕ is as follows:

$$\phi_Q = \text{round}\left(\frac{Q}{2\pi}\phi + 1\right) \cdot \left(\frac{\pi}{Q}\right) \quad (5)$$

As shown in Fig. 2, since quantization is a discretization process, the networks parameters are no longer continuous and differentiable after being quantized, so HQ-D²NN cannot use the back propagation algorithm of deep learning to be optimized. We use Straight-Through-Estimator (STE) technology[24, 25] to solve the problem of non-derivability of quantization functions. Its function is that when the gradient pass encounters a quantization function, STE helps the gradient to skip that function directly, and makes the gradient of the quantization function output to input 1. Namely, $\frac{\partial y}{\partial \Phi}$ is used to replace $\frac{\partial y}{\partial \Phi_Q}$ when calculating the gradient of the error y . Though $\frac{\partial y}{\partial \Phi_Q} \neq \frac{\partial y}{\partial \Phi}$, $\frac{\partial y}{\partial \Phi_Q}$ is on expectation equal to $\frac{\partial y}{\partial \Phi}$ and many related works have

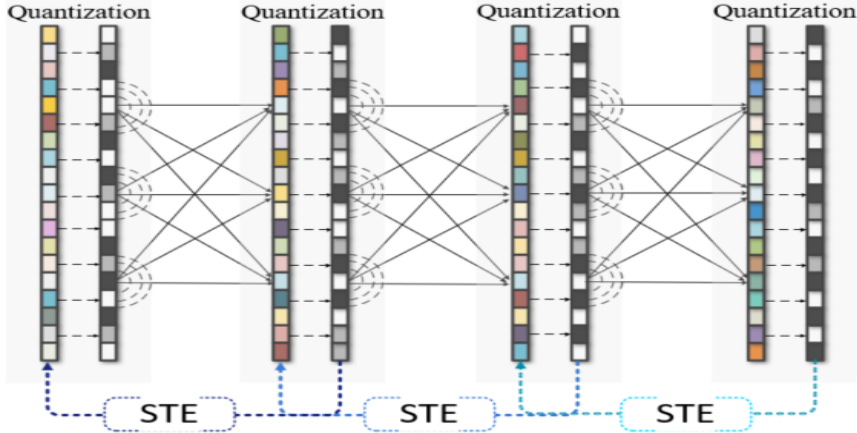


Figure 2: Schematic of HQ₃-D²NN training. Different colors of neurons represent different parameter values.

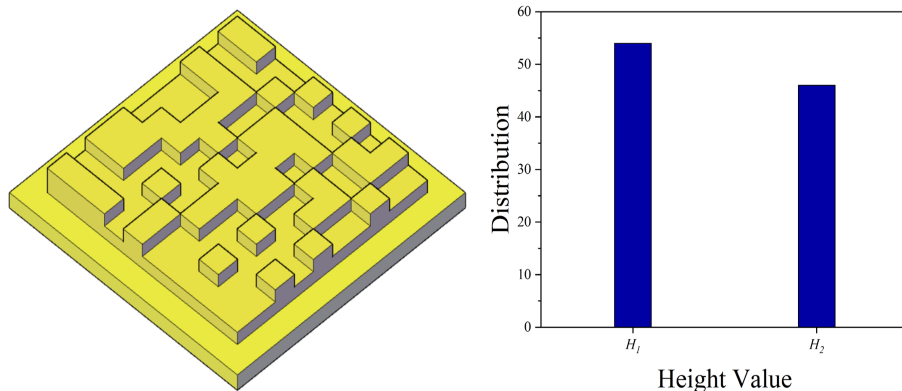
proven that the two have a strong correlation[24, 25], so $\frac{\partial y}{\partial \Phi_Q}$ can be approximately replaced by $\frac{\partial y}{\partial \Phi}$ because we only care about the trend of loss reduction rather than the specific value. Therefore, the neuron parameters of the diffractive networks are constrained to the corresponding quantized values during the forward propagation. After the forward propagation, the networks back propagation based on the output value, and uses STE to fit the quantized values of the neuron parameters to calculate the gradient of the neurons[26]. To further compensate the potential bias introduced by gradient quantized, we introduce an extra noise function $N(Q) = \frac{\sigma}{2^{k-1}}$, where $\sigma \sim Uniform(-0.5, 0.5)$. This design allows the amplitude of the noise to have as much as possible the same amplitude as the quantization error. Where, $d\phi = \frac{\partial y}{\partial \Phi}$, $\max(|d\phi|)$ is taken over all axis of the gradient tensor $d\phi$. The above function first applies an affine transform on the gradient, to map it into [0, 1], and then inverts the transform after quantization. The gradient quantization and error gradient calculation formulas are as follows:

$$f_Q(d\phi) = 2\max(|d\phi|) \cdot [\text{round}\left(\frac{d\phi}{2\max(|d\phi|)} + \frac{1}{2}\right) + N(Q)] - \frac{1}{2} \quad (6)$$

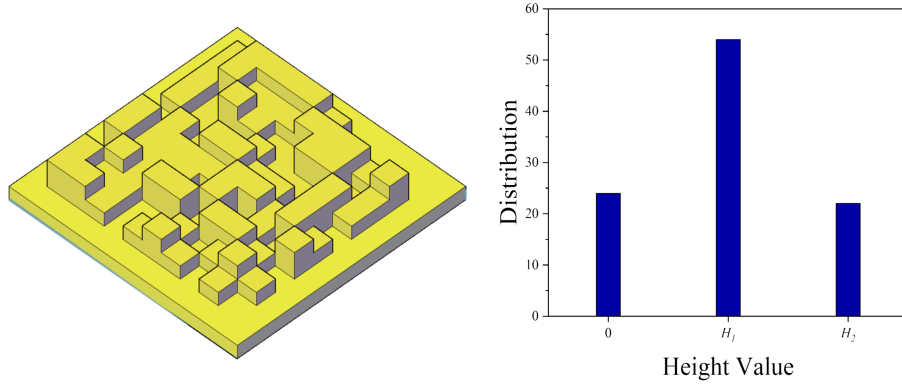
$$\frac{\partial y}{\partial \Phi_Q} = f_Q \cdot [STE\left(\frac{\partial y}{\partial f_Q}\right)] = f_Q\left(\frac{\partial y}{\partial \Phi}\right) \quad (7)$$

Based on the HQ-D²NN structure, we design HQ₂-D²NN, HQ₃-D²NN and HQ₄-D²NN with quantization values of 2, 3 and 4 respectively. The parameter values of HQ₂-D²NN are constrained to $\pi/3$ and $2\pi/3$, the parameter values of HQ₃-D²NN are constrained to 0, $\pi/3$ and $2\pi/3$, and the parameter values of HQ₄-D²NN are constrained to $\pi/4$, $3\pi/4$, $5\pi/4$, and $7\pi/4$. The networks structure and parameter

1
2 distribution of these are shown in Fig. 3 and 4. Where, the quantization functions of
3 HQ₂-D²NN, HQ₃-D²NN and HQ₄-D²NN are formulas (8), (9) and (10) respectively.
4
5
6
7
8
9
10
11
12
13
14
15
16
17



18
19 Figure 3: HQ₂-D²NN structure diagram and phase value distribution. The height of each diffrac-
20 tion grating can only be H_1 or H_2 .
21
22



36
37 Figure 4: HQ₃-D²NN structure diagram and phase value distribution. The height of each diffrac-
38 tion grating can only be H_1 , H_2 or 0.
39
40

$$\Phi_{HQ_2-D^2NN} = \begin{cases} \pi/3, 0 < \Phi < \pi \\ 2\pi/3, \pi < \Phi < 2\pi \end{cases} \quad (8)$$

$$\Phi_{HQ_3-D^2NN} = \begin{cases} \pi/3, 0 < \Phi < \pi/2 \\ 0, \pi/2 < \Phi < 3\pi/2 \\ 2\pi/3, 3\pi/2 < \Phi < 2\pi \end{cases} \quad (9)$$

$$\Phi_{HQ_4-D^2NN} = \begin{cases} \pi/4, 0 < \Phi < \pi/2 \\ 3\pi/4, \pi/2 < \Phi < \pi \\ 5\pi/4, \pi < \Phi < 3\pi/2 \\ 7\pi/4, 3\pi/2 < \Phi < 2\pi \end{cases} \quad (10)$$

53 4. Result and discussion

54
55 We verified the effectiveness of the proposed HQ-D²NN by comparing the per-
56 formance of HQ₂-D²NN, HQ₃-D²NN, HQ₄-D²NN, D²NN and D²NN_{DQ} (After D²NN
57 training is completed, the network parameters are quantized by truncation or ap-
58 proximation.) by conducting two image processing tasks, i.e., the object classifica-
59 tion and imaging. These two tasks respectively correspond to the general classifica-
60 tion and regression machine learning tasks.

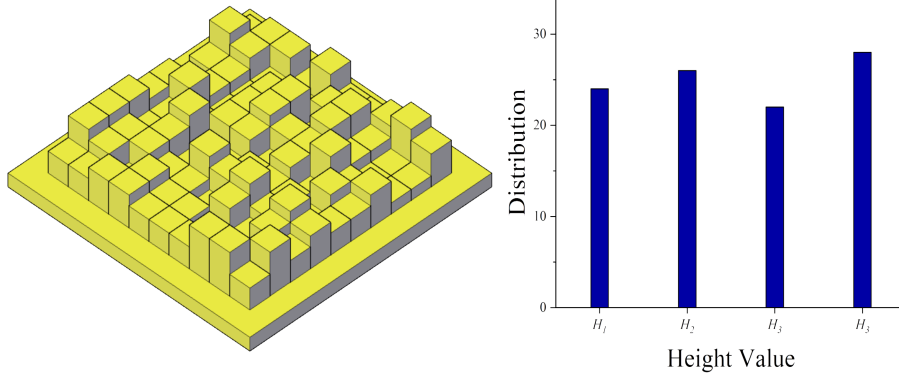


Figure 5: HQ₄-D²NN structure diagram and phase value distribution. The height of each diffraction grating can only be H_1 , H_2 , H_3 or H_4 .

With the aim of proving that HQ-D²NN can still have good performance under low-precision processing conditions, the proposed architecture was validated under the wavelength of 118 μm by setting 50×50 optical neurons on each layer with neuron size of 3 times the wavelength. HQ₂-D²NN, HQ₃-D²NN, HQ₄-D²NN and D²NN have the same structural parameters except for different grating phase value constraints. Each networks has 5 diffraction layers with the axial distance between the successive layers set to be 1cm. With a learning rate of 0.002 and a batch size of 10, the networks was trained by Python version 3.6.0 and TensorFlow framework version 1.4.0 (Google Inc.) and running on a desktop computer (Intel i7-12700H CPU@2.3GHz, 16.0G RAM, NVIDIA GeForce RTX 3050 Ti GPU, and a Microsoft Windows 11 operating system).

In order to use the diffractive networks for object classification, we divide the physical plane of networks output into 10 non-overlapping regions, each of which represents one of the categories in the datasets. The region that exhibits the highest light intensity implies the category of input objects (Fig. 6). We use the MNIST[27] and Fashion-MNIST[28] dataset for image classification task. First, 2000 images are randomly selected from MNIST and Fashion-MNIST respectively and up-sampled to match the networks size. Then these images are randomly divided into 1500 training images, 200 verification images and 300 test images. As shown in Table 1, we compared the classification of D²NN, HQ₄-D²NN, HQ₃-D²NN, HQ₂-D²NN and D²NN_{DQ}. The classification accuracy of HQ₃-D²NN, HQ₄-D²NN and D²NN for MNIST and Fashion-MNIST is similar, both exceeding 95%. HQ₂-D²NN has the lowest accuracy, mainly because the parameter freedom of it is too low and its performance is limited. The convergence diagram and confusion matrix of the test sample are shown in Fig. 6 and 7 respectively.

Table 1: Performance on Digit Classification

	MNIST	Fashion-MNIST
D ² NN	97.7%	95.8%
HQ ₂ -D ² NN	87.5%	83.4%
HQ ₃ -D ² NN	96.9%	95.3%
HQ ₄ -D ² NN	97.35%	95.55%
D ² NN _{DQ}	14.0%	11.4%

By analyzing the convergence rate and performance of HQ-D²NN (The quantization values are 2, 3, and 4 respectively) and D²NN in the MNIST (Fig. 7 and Fig.



Figure 6: Sample experimental results for digit classifier. Energy-dense regions correspond to networks-predicted digital values.

8) and fashion-MNIST (Fig. 9 and Fig. 10) classification tasks, the following conclusions can be drawn: 1) The number of quantization values has a great influence on the performance of HQ-D²NN. It is necessary to select the appropriate number of quantization value for tasks of different complexity (for example, the classification accuracy of HQ-D²NN for fashion-MNIST is lower than that of D²NN when the quantization value is 2, and the training time is longer). 2) When HQ-D²NN selects the appropriate number of quantization value (such as 3 or 4), the performance of the HQ-D²NN is comparable to that of D²NN, but the training time of HQ-D²NN is much less than that of D²NN. This is mainly due to limiting the possible values of each parameter, narrowing the optimization range, and thus saving training time.

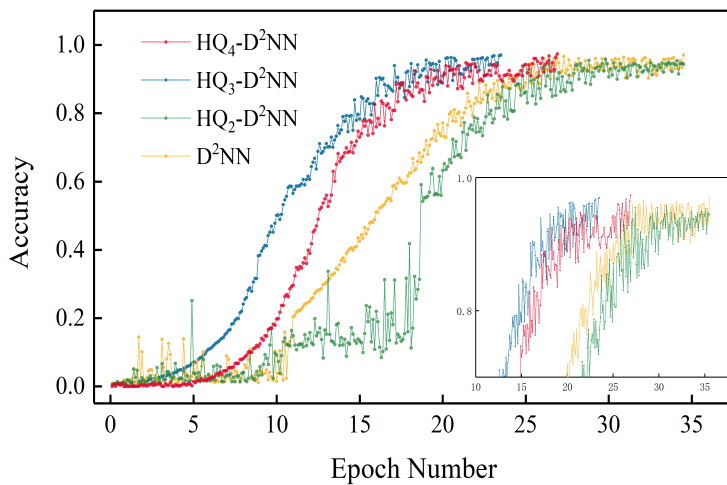


Figure 7: MNIST classification convergence plots.

HQ ₂ -D ² NN											
Label	0	1	2	3	4	5	6	7	8		
Prediction	0	86	0	0	1	0	1	6	1	3	0
1	0	111	0	0	0	0	0	0	2	0	
2	1	6	84	2	8	0	4	4	8	2	
3	1	2	1	59	1	0	5	1	0	2	
4	0	0	0	0	93	0	1	0	1	3	
5	1	1	0	3	0	81	6	0	4	2	
6	0	0	0	0	0	94	0	0	0	0	
7	1	3	0	5	1	0	0	65	0	7	
8	0	1	0	1	7	2	1	0	82	2	
9	1	0	0	0	9	0	0	2	2	86	

HQ ₃ -D ² NN											
Label	0	1	2	3	4	5	6	7	8		
Prediction	0	101	0	0	0	0	0	1	0	1	1
1	0	108	0	3	0	0	0	0	3	0	0
2	1	0	93	1	0	0	0	0	1	0	0
3	0	1	0	96	0	2	0	0	0	0	0
4	0	0	0	0	88	0	0	0	0	1	0
5	1	0	2	2	0	86	1	0	0	0	0
6	2	0	0	0	2	2	91	0	0	0	0
7	0	2	0	0	0	0	0	88	0	1	0
8	2	0	1	0	0	0	0	0	105	0	0
9	1	0	2	0	1	0	0	1	0	0	105

HQ ₄ -D ² NN											
Label	0	1	2	3	4	5	6	7	8		
Prediction	0	97	0	0	1	0	0	1	0	0	0
1	0	94	0	0	2	0	0	1	0	0	0
2	2	0	104	1	0	1	0	0	0	1	0
3	0	0	4	96	3	0	2	0	1	0	0
4	3	0	0	0	95	0	0	1	0	0	0
5	0	2	0	1	0	91	5	0	1	0	0
6	0	0	0	0	2	0	90	0	0	3	0
7	1	0	2	0	0	1	0	92	2	0	0
8	0	2	0	0	2	0	0	4	96	0	0
9	0	0	0	1	0	0	1	0	0	91	0

D ² NN											
Label	0	1	2	3	4	5	6	7	8		
Prediction	0	95	0	0	3	0	0	2	0	0	0
1	0	112	1	0	0	1	0	1	0	0	0
2	3	0	99	0	4	0	0	0	1	0	0
3	0	2	0	90	0	0	0	1	0	0	0
4	2	1	0	6	90	1	0	0	3	2	0
5	0	0	2	3	0	89	2	0	0	0	0
6	0	0	0	0	2	0	90	0	2	0	0
7	1	2	0	6	0	0	0	93	0	3	0
8	0	0	2	1	0	0	1	0	92	0	0
9	0	0	2	0	0	1	0	0	4	93	0

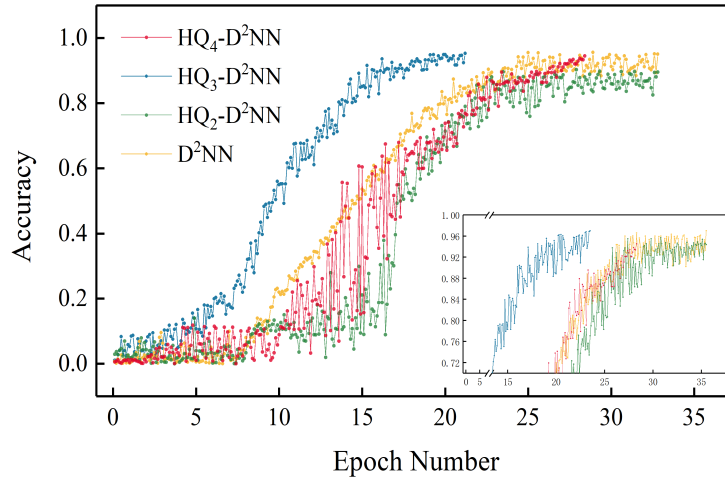
Figure 8: Confusion matrixes of different quantization values of HQ-D²NN for MNIST.

Figure 9: Fashion-MNIST classification convergence plots.

HQ ₂ -D ² NN											
Label	0	1	2	3	4	5	6	7	8		
Prediction	0	99	2	0	1	0	2	2	0	0	0
1	0	97	1	0	0	0	0	0	1	0	0
2	2	0	92	1	1	0	5	1	0	1	0
3	0	1	0	93	0	1	0	1	0	0	0
4	2	0	0	0	91	0	0	0	4	2	0
5	1	0	0	2	0	92	2	0	0	0	0
6	0	1	0	0	2	0	95	0	4	0	0
7	1	0	0	2	0	0	0	91	0	0	0
8	0	0	1	0	0	3	1	0	97	0	0
9	0	0	2	0	1	0	0	2	1	96	0

HQ ₃ -D ² NN											
Label	0	1	2	3	4	5	6	7	8		
Prediction	0	102	2	0	1	0	0	2	0	0	0
1	0	101	1	0	0	1	0	0	0	0	0
2	2	0	92	3	1	0	0	1	0	1	0
3	0	1	0	94	0	0	0	0	0	0	0
4	2	0	0	0	90	0	0	0	2	2	0
5	1	0	2	0	0	92	2	0	0	0	0
6	0	0	0	0	2	0	0	93	0	0	0
7	1	2	0	3	0	2	0	0	90	0	0
8	0	0	1	1	0	0	1	0	103	0	0
9	0	0	2	0	0	1	0	0	2	2	96

HQ ₄ -D ² NN											
Label	0	1	2	3	4	5	6	7	8		
Prediction	0	98	0	0	4	0	0	1	0	0	0
1	0	94	3	0	0	1	0	1	2	0	0
2	2	0	92	1	0	0	3	0	0	0	0
3	0	0	0	95	3	0	0	1	0	0	0
4	1	0	2	0	93	1	0	0	3	0	0
5	1	0	0	0	4	107	0	1	0	0	1
6	0	1	0	1	0	91	0	2	0	0	0
7	2	0	0	0	1	0	7	88	0	0	0
8	0	3	0	0	0	1	0	0	91	1	0
9	0	0	2	0	0	0	0	4	0	0	89

D ² NN											
Label	0	1	2	3	4	5	6	7	8		
Prediction	0	82	4	0	3	0	0	2	0	1	0
1	0	92	0	0	1	1	0	0	3	0	0
2	0	0	90	1	1	0	0	2	0	2	0
3	0	2	7	84	0	3	0	0	3	0	0
4	1	0	0	0	99	0	1	0	0	0	0
5	0	1	0	1	2	90	5	0	3	0	0
6	2	0	3	0	0	0	98	2	0	0	0
7	0	0	2	0	0	0	1	0	90	7	1
8	0	0	0	2	0	0	0	0	2	108	0
9	0	1	0	0	0	4	0	0	0	1	90

Figure 10: Confusion matrixes of different quantization values of HQ-D²NN for Fashion-MNIST.

We also used Fashion-MNIST to verify the capabilities of HQ-D²NN and D²NN in image reconstruction. Compared with MNIST digits, Fashion-MNIST images are generated from real-world objects and contain richer texture information, which makes it an ideal dataset for testing the regression capabilities of HQ-D²NN. In the experiments, we randomly select 90% of the images for training and the rest for testing. In order to reduce processing and manufacturing costs, we set the number of neurons in each layer of the network to 50x50 which size is 4 times the wavelength. Each networks has 5 diffraction layers with the axial distance between the successive layers set to be 200 times the wavelength. The training batch size was set to be 10 and the initial learning rate was set to be 0.002. We show some samples in Fig. 11 for subjective evaluation. As illustrated in the Fig. 11, D²NN_{DQ} reconstructed images are the most distorted and HQ-D²NN with different quantization values such as 2, 3 and 4 both retained a lot of details.

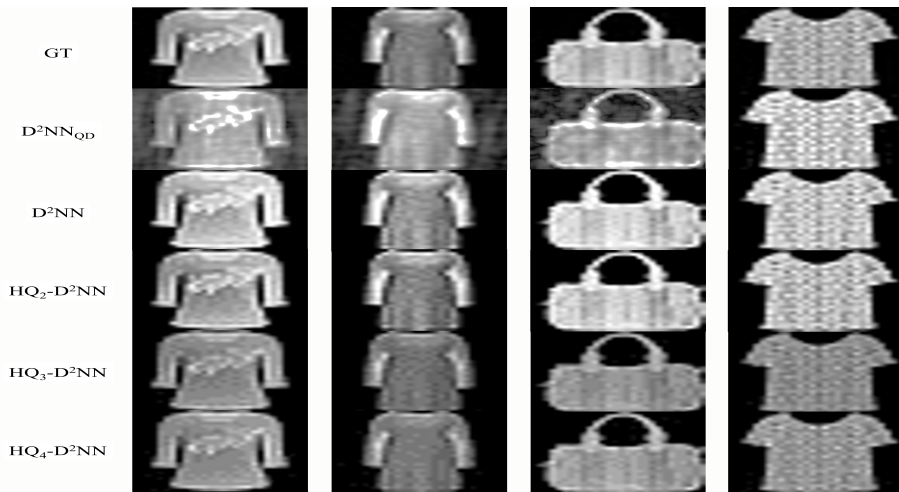


Figure 11: Demonstration for imaging of D²NN, D²NN_{DQ}, HQ-D²NN with different quantization values.

It can be seen from Table 2 that the height quantization of D²NN has little effect on the imaging quality. When the quantization value is selected appropriately, the imaging performance of HQ-D²NN is close to that of D²NN. When the quantization value is higher, the imaging quality of the HQ-D²NN structure is better.

Table 2: Performance on Digit Classification

	PSNR/dB	SSIM
D ² NN	21.2623	0.7403
HQ ₂ -D ² NN	20.4433	0.6683
HQ ₃ -D ² NN	21.4052	0.7396
HQ ₄ -D ² NN	21.1536	0.7350
D ² NN _{DQ}	15.0458	0.4084

To verify the inference capabilities of HQ-D²NN, we compared the imaging performance of HQ-D²NN with different numbers of neurons by changing the diffractive networks size. As shown in Fig. 12 and Fig. 13, the imaging quality of HQ-D²NN gradually improves as the size of the diffractive networks increases. When the number of neurons is small, the performance of HQ-D²NN with different quantization values are quite different. As the number of neurons increases, the performance difference of HQ-D²NN with different quantization values gradually decreases. There-

fore, for HQ-D²NN with lower quantization values, the performance can be improved by increasing the networks size.

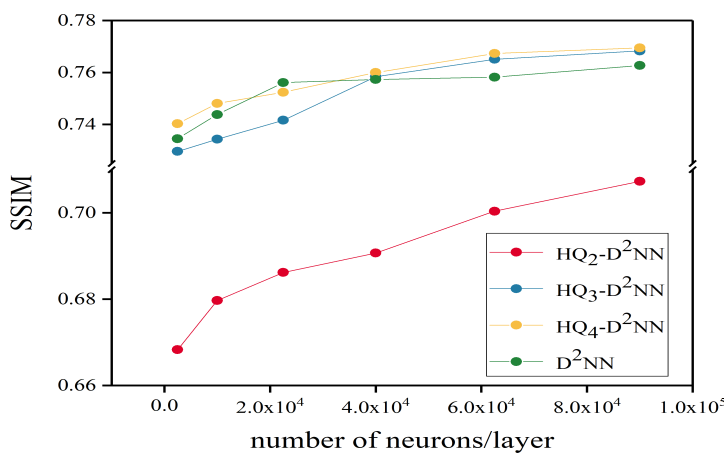


Figure 12: SSIM rate with different number of neurons of diffractive networks with different quantization values.

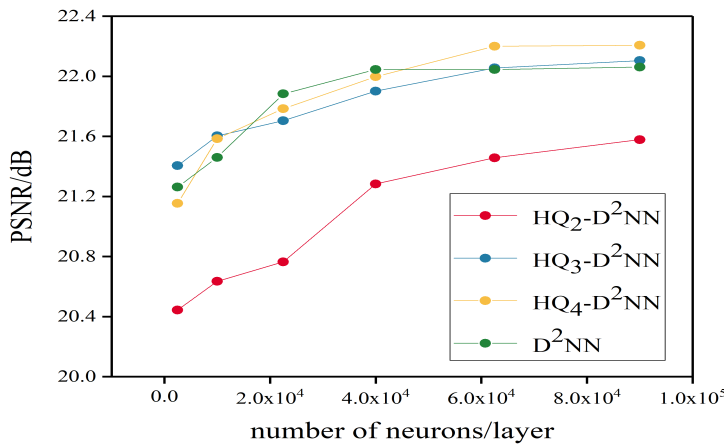


Figure 13: PSNR rate with different number of neurons of diffractive networks with different quantization values.

5. Conclusion

In summary, due to the accuracy and cost limitations of current fabrication technology, we propose a HQ-D²NN, which can change the resolution of the networks structure by setting specific phase module values. Although the accuracy of HQ-D²NN is reduced, the training effect is not worse than that of the D²NN, there are times when the training effect of the HQ-D²NN will even exceed that of the D²NN, because the quantization process introduces noise into the networks, such as dropout, but instead it is a kind of regularisation that can partially avoid the overfitting of the networks. For different tasks and cost requirements, this network can be customized to change the number of quantization values, thereby reducing processing costs.

Funding

National Natural Science Foundation of China (62205046); Natural Science Foundation of Liaoning Province (2023-BS-074); Fundamental Research Funds for the

Central Universities (3132023230); Fundamental Research Funds for the Central Universities; China (Grant No. 2042022dx0001); National Key Research and Development Program of China (2022YFB4301401, 2022YFB4300401); Central level research institutes research special project of China (182310).

Disclosures

The authors declare no conflicts of interest.

Data Availability Statement

Data will be made available on request.

References

- [1] Mnih, V., Kavukcuoglu, K., Silver, D., Rusu, A.A., Veness, J., Bellemare, M.G., Graves, A., Riedmiller, M., Fidjeland, A.K., Ostrovski, G., et al., 2015. Human-level control through deep reinforcement learning. *Nature* 518, 529–533.
- [2] Amoretti, M., Amsler, C., Bonomi, G., Bouchta, A., Bowe, P., Carraro, C., Cesar, C., Charlton, M., Collier, M., Doser, M., et al., 2002. Production and detection of cold antihydrogen atoms. *Nature* 419, 456–459.
- [3] LeCun, Y., Bengio, Y., Hinton, G., 2015. Deep learning. *Nature* 521, 436–444.
- [4] Xu, X., Tan, M., Corcoran, B., Wu, J., Boes, A., Nguyen, T.G., Chu, S.T., Little, B.E., Hicks, D.G., Morandotti, R., et al., 2021. 11 tops photonic convolutional accelerator for optical neural networks. *Nature* 589, 44–51.
- [5] Feldmann, J., Youngblood, N., Karpov, M., Gehring, H., Li, X., Stappers, M., Le Gallo, M., Fu, X., Lukashchuk, A., Raja, A.S., Liu, J., Wright, C.D., Sebastian, A., Kippenberg, T.J., Pernice, W.H.P., Bhaskaran, H., 2021. Parallel convolutional processing using an integrated photonic tensor core. *Nature* 589, 52–58. doi:10.1038/s41586-020-03070-1.
- [6] Zhou, H., Dong, J., Cheng, J., Dong, W., Huang, C., Shen, Y., Zhang, Q., Gu, M., Qian, C., Chen, H., Ruan, Z., Zhang, X., 2022. Photonic matrix multiplication lights up photonic accelerator and beyond. *Light: Science & Applications* 11, 30. doi:10.1038/s41377-022-00717-8.
- [7] Xu, Z., Yuan, X., Zhou, T., Fang, L., 2022. A multichannel optical computing architecture for advanced machine vision. *Light: Science & Applications* 11, 255. doi:10.1038/s41377-022-00945-y.
- [8] Luo, X., Hu, Y., Ou, X., Li, X., Lai, J., Liu, N., Cheng, X., Pan, A., Duan, H., 2022. Metasurface-enabled on-chip multiplexed diffractive neural networks in the visible. *Light: Science& Applications* 11, 158. doi:10.1038/s41377-022-00844-2.
- [9] Shainline, J.M., Buckley, S.M., Mirin, R.P., Nam, S.W., 2017. Superconducting optoelectronic circuits for neuromorphic computing. *Physical Review Applied* 7, 034013. doi:10.1103/PhysRevApplied.7.034013.
- [10] Shen, Y., Harris, N.C., Skirlo, S., Prabhu, M., Baehr-Jones, T., Hochberg, M., Sun, X., Zhao, S., Larochelle, H., Englund, D., Soljačić, M., 2017. Deep learning with coherent nanophotonic circuits. *Nature Photonics* 11, 441–446. doi:10.1038/nphoton.2017.93.

- [1] Zhao, Q., Hao, S., Wang, Y., Wang, L., Xu, C., 2019. Orbital angular momentum detection based on diffractive deep neural network. *Optics Communications* 443, 245–249.
- [2] Liao, K., Chen, Y., Yu, Z., Hu, X., Wang, X., Lu, C., Lin, H., Du, Q., Hu, J., Gong, Q., 2021. All-optical computing based on convolutional neural networks. *Opto-Electronic Advances* 4, 200060.
- [3] Huang, C., Fujisawa, S., de Lima, T.F., Tait, A.N., Blow, E.C., Tian, Y., Bilodeau, S., Jha, A., Yaman, F., Peng, H.T., et al., 2021. A silicon photonic-electronic neural network for fibre nonlinearity compensation. *Nature Electronics* 4, 837–844.
- [4] Xu, X., Ren, G., Feleppa, T., Liu, X., Boes, A., Mitchell, A., Lowery, 2022. Self-calibrating programmable photonic integrated circuits. *Nature Photonics* 16, 595–602.
- [5] Lin, X., Rivenson, Y., Yardimci, N.T., Veli, M., Luo, Y., Jarrahi, M., Ozcan, A., 2018. All-optical machine learning using diffractive deep neural networks. *Science* 361, 1004–1008.
- [6] Yan, T., Wu, J., Zhou, T., Xie, H., Xu, F., Fan, J., Fang, L., Lin, X., Dai, Q., 2019. Fourier-space diffractive deep neural network. *Physical review letters* 123, 023901.
- [7] Dou, H., Deng, Y., Yan, T., Wu, H., Lin, X., Dai, Q., 2020. Residual d 2 nm: training diffractive deep neural networks via learnable light shortcuts. *Opt. Lett.* 45, 2688–2691.
- [8] Chen, Y., Zhu, Y., Britton, W.A., Negro, L.D., 2022. Inverse design of ultra-compact multi-focal optical devices by diffractive neural networks. *Opt. Lett.* 47, 2842–2845. doi:10.1364/OL.460186.
- [9] Shi, J., Chen, Y., Zhang, X., 2022. Broad-spectrum diffractive network via ensemble learning. *Opt. Lett.* 47, 605–608. doi:10.1364/OL.440421.
- [10] Xiao, Y.L., Li, S., Situ, G., You, Z., 2021. Optical random phase dropout in a diffractive deep neural network. *Opt. Lett.* 46, 5260–5263. doi:10.1364/OL.428761.
- [11] Song, M., Li, R., Wang, J., 2023. Only frequency domain diffractive deep neural networks. *Applied Optics* 62, 1082–1087.
- [12] Song, M., Li, R., Guo, R., Ding, G., Wang, Y., Wang, J., 2022. Single image dehazing algorithm based on optical diffraction deep neural networks. *Optics Express* 30, 24394–24406.
- [13] Shi, J., Chen, M., Wei, D., Hu, C., Luo, J., Wang, H., Zhang, X., Xie, C., 2020. Anti-noise diffractive neural network for constructing an intelligent imaging detector array. *Optics Express* 28, 37686–37699.
- [14] Courbariaux, M., Hubara, I., Soudry, D., El-Yaniv, R., Bengio, Y., 2016. Binarized neural networks: Training deep neural networks with weights and activations constrained to + 1 or -1. *arXiv preprint arXiv:1602.02830*.

- 1
2 [25] Li, F., Liu, B., Wang, X., Zhang, B., Yan, J., 2016. Ternary weight networks.
3 arXiv preprint arXiv:1605.04711 .
4
5 [26] Zhou, S., Wu, Y., Ni, Z., Zhou, X., Wen, H., Zou, Y., 2016. Dorefa-net: Training
6 low bitwidth convolutional neural networks with low bitwidth gradients. arXiv
7 preprint arXiv:1606.06160 .
8
9 [27] Lecun, Y., Bottou, L., Bengio, Y., Haffner, P., 1998. Gradient-based learning
10 applied to document recognition. Proceedings of the IEEE 86, 2278–2324.
11 doi:10.1109/5.726791 .
12
13 [28] Xiao, H., Rasul, K., Vollgraf, R., 2017. Fashion-mnist: a novel image dataset for
14 benchmarking machine learning algorithms. arXiv preprint arXiv:1708.07747 .
15
16
17
18
19
20
21
22
23
24
25
26
27
28
29
30
31
32
33
34
35
36
37
38
39
40
41
42
43
44
45
46
47
48
49
50
51
52
53
54
55
56
57
58
59
60